Virtual metabolic human dynamic model for pathological analysis and therapy design for diabetes

Hiroyuki Kurata

Department of Bioscience and Bioinformatics, Kyushu Institute of Technology,

680-4 Kawazu, Iizuka, Fukuoka 820-8502, Japan.

kurata@bio.kyutech.ac.jp

ABSTRACT

A virtual metabolic human model is a valuable complement to experimental biology and clinical studies, because *in vivo* research involves serious ethical and technical issues. A whole-body dynamic model is required not only to reproduce a variety of physiological and metabolic functions, but also to analyze pathology and design drugs. I first proposed a virtual metabolic human model, a multi-organ and multi-scale kinetic model of the whole-body metabolism that formulates the reactions of enzymes and transporters with the regulation of enzyme activities and hormonal actions under prandial and rest conditions. To accurately simulate metabolic changes and robustness, the model incorporates nucleotide cofactors that are critically responsible for global feedback regulations to adapt to metabolic changes. The model predicted a two-phase hepatic fatty acid production that consists of the synthesis of malonyl-CoA and the NADPH-dependent synthesis of fatty acid. The model performed pathological analysis of type 2 diabetes. I divided type 2 diabetes into specific disorders of steatosis, β cell dysfunction and insulin resistance for each organ, and analyzed the effect of the individual disorders on the dynamics of plasma glucose (hyperglycemia) and hepatic TG (steatosis). The model suggested that a chronic or irreversible change in hepatic TG accumulation plays a critical role in disease progression. The model predicted a glycerol kinase inhibitor to be a new medicine for type 2 diabetes, because it not only decreased hepatic TG but also reduced plasma glucose, unexpectedly. The model also enabled us to rationally design combination therapy.

INTRODUCTION

Virtual physiological human is a final goal for synthetic biology, systems biology and bioinformatics, which greatly contributes to advances in medicine and life science. Many scientists have raised concepts and plans of the computer model of human physiology, and are developing computational frameworks on genome-scale gene networks and whole-body scale omics data (*1, 2*). In 2019, the virtual metabolic human database has been presented to facilitate computational modeling by linking genome-scale networks of human metabolism to diseases and nutrition (*3*). On the other hand, multi-scale, large-scale dynamic models have been extensively developed for human metabolism (*4-11*). A virtual metabolic human model is highly expected as a core model toward the virtual physiological human.

Metabolism plays a critical role in human health and diseases (*12*). Perturbation of genetics and changes in lifestyle habitats, including excess sugar, excess fat and inactivity, result in the development and progression of complex metabolic diseases, such as hyperglycemia, hyperlipidemia, obesity, non-alcoholic fatty liver disease (NAFLD) (*13, 14*) and diabetes(*13, 15-17*). A systems approach is necessary to elucidate the molecular mechanisms causing such metabolic dysfunctions and to propose the strategies for the prevention and treatment of them (*18*). Since *in vivo* studies of human metabolism are hampered with serious ethical and technical problems, computational models are required to complement the *in vivo* studies (*19-21*).

So far many mathematical models have simulated human metabolism. Early models extensively investigated glucose-insulin metabolism to analyze the effect of insulin secretion on glucose homeostasis (*22*). They used the compartment models that regarded particular metabolites as the representatives responsible for their associated functions such as glycolysis, gluconeogenesis, glycogenolysis, glycogenesis, and triglyceride (TG) synthesis/degradation. Compartment models simulated the glucagon/insulin-controlled glucose homeostasis by linking liver to other organ compartments (*23-25*), and suggested the mechanisms by which changes in a ratio of carbohydrate to lipid alter hepatic TG synthesis through insulin action (*26*) and generate different types of diabetes (*27*).

Since those compartment models were the coarse-grained models, their applications were limited to an understanding of the specific functions. To overcome this limitation, biochemistry-based models were constructed that assigned a rate equation to each metabolic reaction within a cell of liver and skeletal muscle while considering allosteric effectors, enzyme activity regulation, and hormone-dependent reversible phosphorylation (*5, 6, 11*). The kinetics were measured by means of *in vitro* assays. In 2019 Berndt et al developed a genome-scale, detailed kinetic model of hepatic cells that formulated thousands of enzymes, transporters, and hormone-dependent regulations. It is the largest kinetic model for all the models (*11*).

Those biochemistry-based models pay attention to cells of liver and skeletal muscle, while it is important to consider the rest of the human body because organs are tightly connected with each other through blood (*7, 8, 28*). Xu et al integrated hepatic glycogen regulation with extra-hepatic fuel metabolism under prandial and rest conditions in the

whole-body context (*28*). Sluka et al. proposed a liver-centric model for acetaminophen pharmacology and metabolism in the whole-body context (*7*). They integrated three scale modules of enzyme reactions within a cell, physiologically based pharmacokinetics of acetaminophen at organs, and its distribution at the whole-body level. Ashworth et al developed a spatial kinetic model of liver glucose and lipid metabolism and treated the sinusoidal tissue units instead of the single hepatocyte (*8*). They identified critical differences between periportal and pericentral cells, indicating high susceptibility to pericentral steatosis during the development of steatosis. Berndt et al. also presented a dynamic model of the sinusoidal tissue units to suggest that structural properties, enzymatic properties and regional blood flows are equally important for an understanding of liver functionality (*9, 10*). Kim et al proposed a whole-body computational model to simulate hormonal control over plasma glucose and TG during physical exercise (*4*). They decomposed the whole body into seven organs, assigned each major metabolite within organs to an ordinary differential equation. Palumbo et al. added details of subjects' characteristics to the Kim's model to simulate the effects on personal metabolic homeostasis during exercise (*29*).

Construction of the whole-body metabolism models has just started, but their application is still limited due to lack of comprehensive and systematic mechanisms. At present a virtual metabolic human model that integrates multi-scale, comprehensive molecular mechanisms is expected not only to reproduce a variety of physiological and metabolic functions, but also to analyze pathology and design therapy. To achieve these requirements, I have developed a multi-organ, multi-scale kinetic model of the whole-body metabolism that accurately simulates the dynamics in key metabolites of glucose, lactate, alanine, glycerol, glycogen, free fatty acid (FFA) and TG under prandial and rest conditions, without impairing any essential reaction pathways of carbohydrates and lipids. To enhance the accuracy and applicability, the model incorporated nucleotide cofactors that are critically responsible for global metabolic regulations and energy balance. Use of the model performed pathological analysis of steatosis, hyperglycemia, hyperinsulinemia and diabetes, discovered a novel medicine for type 2 diabetes, and proposed a combination therapy.

METHODS

Homeostasis of metabolites in blood

Glucose and hormone

Plasma glucose in human is controlled with a set-point of 5 mM by hormones of insulin and glucagon (*12*). Insulin is the only hormone that decreases the plasma glucose concentration, while multiple glucose increasing hormones are known. Glucagon is a counter partner of insulin. The plasma concentrations of insulin and glucagon directly respond to changes in plasma glucose. The plasma glucose concentration is maintained in a narrow range between a minimum value of 3 mM after prolonged fasting or exercise and a maximum value of 9 mM after a meal (*30*). Glucose enters blood in three ways: absorption from the intestine, glycogenolysis in liver, and gluconeogenesis in liver and kidney. After an overnight fast, 95% of glucose production comes from liver (*4*). Liver produces glucose through glycogenolysis and gluconeogenesis with almost equal

contribution at rest. Lactate, pyruvate, alanine and glycerol are the major gluconeogenic precursors. 50% of glucose at rest is utilized by brain, while skeletal muscle uses 20%. The gastrointestinal (GI) tract consumes only 10% of glucose. The organs except brain use FFA as metabolic fuels to save glucose.

Lactate, pyruvate and alanine

Liver and heart primarily consume plasma lactate, while skeletal muscle, adipose tissue and other tissues, including inactive upper body muscles and red blood cells, produce lactate. Pyruvate exchange occurs primarily between skeletal muscle and other tissues. Plasma pyruvate concentration is very small or negligible. Only liver consumes amino acids, especially alanine, for gluconeogenesis, while skeletal muscle is the main source of alanine and the inactive muscle in other tissues is an additional source.

FFA, glycerol and TG

FFA and glycerol are mainly produced from lipolysis of TG in adipose tissue. Liver uptakes FFA from blood and utilizes FFA as a main fuel. A half of the liver-taken FFA is oxidized; the half is re-esterified into TG (*4, 12*). Since adipose tissue lacks glycerol phosphorylase, lipolysis-produced glycerol is not utilized for TG synthesis in adipose tissue. Liver uptakes the glycerol released from adipose tissue and utilize it as a gluconeogenic precursor, i.e., a substrate for TG synthesis.

Ketone body

Ketone bodies including β-hydroxybutyrate (Bhb) are synthesized from acetyl-CoA produced through β-oxidation. Synthesis of ketone bodies are stimulated mainly by glucagon in liver under a fasted condition. Ketone bodies are utilized exclusively by brain.

Metabolic reactions of each organ

Liver and pancreas

Liver plays a central role in buffering or controlling plasma glucose. Switching between the glucose utilization (glycolysis and glycogenesis) and glucose production (gluconeogenesis and glycogenolysis) is dependent on the plasma glucose level. The glucose utilization occurs at glucose concentration exceeding a critical threshold value; the glucose production occurs below the critical concentration. Insulin alters the phosphorylation state of multiple key interconvertible enzymes of hexokinase (HK), glycogen synthase (GS), glycogen phosphorylase (GP), phosphofructokinase (PFK), fructose-1,6-bisphosphatase (FBP), pyruvate kinase (PK) and pyruvate dehydrogenase (PDH) to shift a remarkable metabolic state. Liver temporally stores substantial amounts of glucose as glycogen, synthesizes glucose from small carbohydrates, including lactate, pyruvate, glycerol and alanine, and converts excess glucose into FFA. It also synthesizes TG and cholesterol and secretes them into blood. Under a fasted condition, liver synthesizes Bhb from acetyl-CoA as a metabolic fuel for brain. In pancreas β cells serve as a controller of insulin synthesis and release in response to a plasma glucose concentration.

Skeletal muscle and heart

Insulin activates glucose transporter 4 (GLUT4) in skeletal muscle to uptake glucose and to accumulate glycogen. To control substantially glucose uptake rates, a few key enzymes of HK, GS, and PDH are activated (*31, 32*). In this study skeletal muscle represents the lean muscles in the lower extremity. Skeletal muscle uptakes FFA as fuels and releases

lactate and alanine into blood. Heart consists of specialized muscle cells (cardiomyocytes) and constantly uptakes metabolic fuels, including glucose, lactate, and FFA to generate ATP to maintain contractile function without any fatigue. In contrast to skeletal muscle, GLUT1, which is not controlled by insulin, is dominant. The major metabolic fuel for the heart is FFA.

Adipose tissue and GI tract

Adipose tissues are producers and reservoirs of TG. Plasma TG is degraded by lipase on the adipose tissue surface into FFA and glycerol. FFA enters the adipose cells; glycerol returns to blood. Within adipose tissue, FFA and glycerol-3-P are synthesized into TG. Since adipose tissue lacks glycerol kinase, glycerol-3-P comes just from glucose-derived glycelaldehyde-3-phosphate (GAP). Insulin activates the TG synthesis and lipase reaction, facilitating TG accumulation. GI tract includes the splanchnic region (stomach, spleen, intestines) except liver. It utilizes glucose, accumulates TG, and releases FFA and glycerol into blood.

Brain and other tissues

Brain constantly takes only glucose and Bhb as metabolic fuels, neither utilizes FFA nor TG, because the blood-brain barrier prevents such large-size molecules from entering brain. It has Bhb degradation pathways to degrade Bhb into acetyl-CoA for energy. The other tissue compartment includes kidney, upper extremity muscles, and the rest of tissues.

Mathematical model

Model overview

A schematic diagram of the whole body is shown in **Figure 1**. I constructed the union of all the metabolic networks of the organs (**Figure 2**). I lumped associated enzyme reactions into a chemical reaction equation based on Recon2.2 (*33*). Each organ metabolic network was built by selecting organ-specific reactions from the union network. The whole-body model formulates the metabolic enzyme and transporter reactions with regulation of enzyme activities and hormonal actions for all the organs. A meal of glucose and TG is inputted into blood through the GI tract. The model focuses on insulin hormone, assuming that glucagon effect is approximately opposite to insulin. Note that detailed kinetics of glucagon *in vivo* remains to be measured (*34, 35*). The model takes account for glucose, lactate, glycerol, alanine, Bhb, TG, FFA and insulin in blood, assuming the perfect mixing that there is no spatial gradient of metabolites, oxygen and carbon dioxide in each organ. In this study alanine represents the gluconeogenic amino acids and Bhb represents ketone bodies. Notably, the nucleotide cofactors of ATP, GTP, UTP, NADH, NADPH, and $FADH_2$ are incorporated to reflect realistic metabolic changes. The resultant kinetic model consists of 217 reaction rate equations, 147 ordinary differential equations (ODEs) for metabolites, and 1132 kinetic parameter constants, as shown in **Supplemental Equation**, **Supplemental Table S1**, and **Supplemental Table S2**. Abbreviations of the kinetic parameter constants are defined in **Supplemental Table S3**. The differential equations are integrated with ode15s (MATLAB R2019a, Mathworks) to simulate their dynamics.

Module decomposition

A divide and conquer strategy is employed for model construction (*36, 37*). The whole body is decomposed into blood (B) and eight distinct tissue/organ modules (**Figure 1**): liver (L), skeletal muscle (M) adipose tissue (A), GI tract (G), heart (H), brain (N),

pancreas (P), and other tissues (T). Blood acts as the principal transport/exchange medium for metabolites between the different organs. Glucose and TG are inputted to blood through the GI tract, following ingestion of a meal (**Supplemental Equations S1, S2**). Insulin secretion from pancreas is controlled by plasma glucose and FFA concentrations (**Supplemental Equations S4, S5**). Pancreas is simplified as an insulin controller. In liver, many rate equations are derived from several previous works (*4, 8, 10, 11, 25*). I lump multiple associated enzyme reactions and simplify signal transduction pathways including glucose-controlled insulin secretion, phosphorylation of metabolic enzymes, and gene regulations by carbohydrate responsive element binding protein (ChREBP) and sterol-regulatory element binding protein 1c (SREBP-1c). When no experimental rate equation is available, I derive plain Michaelis-Menten type equations based on chemical reaction equations and then estimate the value of Vmax of rate equations. The parameter estimation is carried by genetic algorithms (*38, 39*) so that the model reproduces the experimental transport/exchange fluxes at rest between blood and each organ (*4*) without changing the experimental values of the Michaelis and dissociation constants. In the other organs, where little measured kinetic data is available, I estimate Vmax of enzyme reactions so as to reproduce the experimental transport fluxes at rest (*4*), while fixing the experimental values the Michaelis and dissociation constants. I assume that gene expression profiles depend on organs but the employed enzymes are common to all the organs. The other tissue has no specific regulation.

Module assembly

I combine all the organ modules. To connect blood to each organ, I define α_X and β_X $(X = L, M, A, G, H)$ as the insulin and glucagon factors for each organ, respectively, which alters the activity of insulin- and glucagon-controlled enzymes (**Equations S7-16**). Organs of B, N, P, and T do not have the insulin/glucagon factors. I connect the liver module to the blood module. Subsequently, I add the skeletal muscle, adipose tissue, GI, heart and brain modules. The values of the insulin-related kinetic parameters are estimated so that the model can reproduce the experimental time course data of plasma insulin, plasma glucose, plasma lactate (*40*), plasma FFA, hepatic glycogen (*41*), and plasma TG (*42*).

Dynamic sensitivity analysis

To investigate the robustness of the model, the relative change of metabolite concentrations with respect to a change in a kinetic constant were evaluated. Sensitivity analysis explores some mechanisms by which a system of interest generates robustness and remarkable changes (*43*). The dynamic sensitivity of target parameter y with respect to a change in specific constant parameter p is given by:

$$Sensitivity = \frac{\Delta y}{\Delta p}\frac{p}{y}.$$

In this study, I changed each of parameter constants by 1.1-fold and simulated the metabolite concentrations after 10 h.

Pathological analysis

A long-term excess supply of glucose develops steatosis, lipotoxicity, or ectopic TG accumulation by increasing synthesis of ChREBP, a transcription factor whose expression

is more exclusively regulated by sugars than insulin (*31, 32, 44*). It also leads to the synthesis of SREBP-1c, which is stimulated by insulin under metabolically normal conditions. In steatosis, the activities of enzymes regarding *de novo* lipogenesis (DNL) (synthesis from acetyl-CoA to TG) and cholesterol synthesis abnormally increase in liver. Steatosis or ectopic TG accumulation can cause metabolic diseases, such as hyperglycemia, hyperlipidemia, hyperinsulinemia, obesity, NAFLD and type 2 diabetes (*14, 45-47*). Chronic exposure to high plasma glucose and obesity, leading to oxidative stress and inflammation, induce changes in the regulation of gene expression that converge on impaired glucose-stimulated insulin secretion (*48, 49*) and insulin resistance (IR). Specifically, a lipid metabolite of diacylglycerol (DAG) activates protein kinase C isoforms (PKCs), impairing insulin signaling in organs (*16, 50*). β cell dysfunction in pancreas suppresses glucose-stimulated insulin secretion.

Individual disorder decomposition

While complex mechanisms of metabolic diseases may not be exactly defined, I conveniently decomposed the diseases into individual disorders to perform pathological analysis. I decomposed the diabetes into steatosis, β cell dysfunction, and IR. Steatosis is the underlying disease. β Cell dysfunction of pancreas is a major cause of shifting a set-point of plasma glucose concentration (*15, 50*). IR is further classified with respect to each organ of liver, skeletal muscle, and adipose tissue. IR of each organ is also a major cause. To build a steatosis model, I increased the values of kinetic parameters regarding the DNL and cholesterol synthesis in liver (Vmax_accoat_Accoa_LM_LC, Vmax_lipog1_Accoa_LC, Vmax_lipog2_Malcoa_L, Vmax_tgsyn_FFA_L, Vmax_cholsyn1_Accoa_LC) by 2-fold. β cell dysfunction was represented by multiplying Km_inssyn_Glc_B by 1.5-fold. The IR for liver, skeletal muscle, and adipose tissue, denoted by IR_L, IR_M, and IR_A, were represented by multiplying Km_Ins_B_L, and Km_Ins_B_M, and Km_Ins_B_A by 1.5-fold, respectively.

Diabetes reconstruction

Type 2 diabetes consists of steatosis, β cell dysfunction and IR (*13, 15, 17*). I built three types of type 2 diabetes to analyze the effect of IR on disease progression. The first type is the model that consists of steatosis, β cell dysfunction, and IR_M; the second one is the model that consists of steatosis, β cell dysfunction, IR_M and IR_A; the third one is the model that consists of steatosis, β cell dysfunction, IR_L, IR_M and IR_A. Type 1 diabetes, once known as juvenile diabetes or insulin-dependent diabetes, is the extreme case of β cell dysfunction in which pancreas produces little or no insulin. Differing from the type 2 diseases, type 1 diabetes results from genetic defects or some viruses and it has no cure. To build a type 2 diabetes model, β cell dysfunction, IR_L, IR_M or IR_A was added to the steatosis model. Specifically, I increased the values of Km_inssyn_Glc_B, Km_Ins_B_L, Km_Ins_B_M, and Km_Ins_B_A by 1.5-fold, respectively.

Medication analysis

I used three types of widely prescribed type 2 diabetes medicines: sulfonylurea, metformin and thiazolidinedione to perform medication analysis. In addition to the three medicines, a glycerol kinase inhibitor was used to inhibit TG synthesis (*51*). Sulfonylurea promotes insulin secretion by pancreas (*52*). Metformin is active in the suppression of hepatic gluconeogenesis. (DeFronzo et al 1991; Stumvoll et al 1995) (*46*). Specifically, it

suppresses LDH in liver, accompanied by lactic acidosis (*53*). It also activates AMP-activated protein kinase (AMPK) that regulates energy homeostasis (*53, 54*) or activate β-oxidation. Thiazolidinediones are a family of drugs that have been used in the treatment of type 2 diabetes since the late 1990s (*46*). The thiazolidinedione derivatives, pioglitazone and rosiglitazone, are synthetic ligands for peroxisome proliferative-activated receptor γ (PPARγ) that improve insulin sensitivity. PPARγ is mainly expressed in adipose tissue; PPARγ agonists promote adipocyte differentiation and promote the FFA uptake and storage in subcutaneous adipose tissue rather than visceral sites (*55*). In this study, for inhibition the corresponding kinetic rate constant was set to zero; for activation the corresponding kinetic rate constant was multiplied by 2. Specifically, sulfonylurea multiples Vmax_inssyn_Glc_B by 2. Metformin reduces Vmax_ldh_Pyr_L to zero and multiplies Vmax_boxid_FFA_L by 2. Thiazolidinedione multiplies Vmax_tgsyn_FFA_A by 2. A

Experimental data and subject

The model targets a healthy young adult man with 70kg body weight. A single meal consists of 100 g glucose and 33 g TG. The model employs the experimental transport/exchange fluxes at rest between blood and each organ (*4*) and the experimental time course data of plasma insulin, plasma glucose, plasma lactate (*40*), plasma FFA, liver glycogen (*41*), plasma TG (*42*), and plasma ketone body (*56*).

RESULTS

Model validation by experimental data

The proposed kinetic model simulated the time course of plasma glucose and insulin concentrations after an overnight fast and following a single meal of 100 g glucose and 33 g TG, as shown in **Figure 3**. The plasma glucose concentration increased to a peak around 60 min, then decreased to approximately 5 mM. An increase in plasma glucose triggered the insulin secretion from pancreas to enhance the uptake of plasma glucose by the organs of liver, skeletal muscle, GI, and adipose tissue. The plasma insulin concentration greatly increased to a peak, which was caused by an increase in plasma glucose, and then decreased with a decrease in plasma glucose. In liver and skeletal muscle, the glycogen concentration increased due to insulin action after a meal. At rest, liver glycogen was degraded into glucose (glyocogenolysis), which was released into blood. Skeletal muscle glycogen remained to be degraded, as suggested by (*57*). Plasma lactate increased to a peak after the meal and then decreased. Skeletal muscle and adipose tissue converted a part of the utilized glucose into lactate and released it into blood. Liver utilized plasma lactate to synthesize glucose at rest (gluconeogenesis). Insulin dramatically changed the liver status between glucose utilization and production.

Plasma FFA decreased after the meal, showing a dump, and then gradually increased. In adipose tissue, insulin induced TG synthesis from FFA and glycerol-3-P after the meal, which decreased the release of FFA from adipose tissue. On the other hand, insulin hardly affected the uptake of FFA by liver and skeletal muscle. Consequently, plasma FFA decreased soon after a meal. Plasma TG, ingredient of chylomicrons, slowly increased after a meal, and then decreased. Plasma TG was absorbed mainly by adipose tissue.

As shown in **Figure 4**, the simulated exchange fluxes between each organ and blood at rest were consistent with the experimental data. At rest, skeletal muscle released alanine and lactate; adipose tissue released glycerol and lactate. Liver utilized the three carbon metabolites of lactate, glycerol and alanine to synthesize glucose and released it into blood, indicating that liver recycled the three metabolites into glucose through gluconeogenesis. I confirmed that utilized glycerol was converted to GAP through glycerol-3-P (GRP) in liver (data not shown), indicating that plasma glycerol is used for gluconeogenesis. The model reproduced the glucose-lactate/glycerol/alanine cycles. Liver synthesized TG and cholesterol and then released them into blood. Heart utilized glucose, lactate, and FFA. GI utilized glucose and degraded TG storage into plasma FFA and glycerol. Adipose tissue utilized glucose and TG; it released lactate, FFA and glycerol. Brain exclusively utilized plasma glucose.

Discrepancy between experimental data and simulation

I illustrated some discrepancies between experimental data and simulation. The simulated insulin pulse was sharper than the experimental pulse with a long tail (**Figure 3**). While the simulated glycogen concentration in liver increased to a peak 1 h after the glucose peak, the duration achieving the peak was shorter than that of the experimental data (4-6h). In other words, the simulated glycogen synthesis was faster than experimental data. In addition, the simulated glycogen decrease more rapidly than experimental data. While the simulated plasma lactate increased to a peak at 2 h following the glucose peak, the duration (2h) achieving the peak was longer than the experimental lactate data.

Feature reproduction

The proposed model simulated the switching function between DNL and Bhb synthesis with respect to pyruvate in liver, as shown in **Figure 5**. A high concentration of pyruvate increased DNL flux; a very low concentration of pyruvate induced Bhb synthesis flux. The β-oxidation flux gradually decreased with an increase in pyruvate, while the DNL flux and PDH flux increased. It indicates the typical, reverse relationships between DNL and β-oxidation and between glycolysis and β-oxidation (*12*).

Dynamic sensitivity analysis

I performed dynamic sensitivity analysis of metabolite concentrations with respect to specific kinetic parameters, as shown in **Figure 6**. The plasma glucose level was highly robust with respect to changes in the kinetic parameters except the insulin-related parameters including Km_inssyn_Glc_B, Km_Ins_B_L and Km_Ins_B_M. The set-point of plasma glucose is controlled just by insulin. Km_inssyn_Glc_B, which determines glucose-stimulated insulin secretion, was the most effective parameter that altered the set-point of plasma glucose. Km_Ins_B_L and Km_Ins_B_M, which determine insulin-stimulated glucose uptake, were the second and third critical parameters, respectively. Km_Ins_B_A hardly affected the set-point, because the glucose uptake rate of adipose tissue was much less than that by skeletal muscle. In addition to the insulin-related parameters, nucleotide synthesis-related parameters showed high sensitivities of some metabolites.

Prediction of hidden mechanisms

As shown in **Figure 7**, the proposed model suggested two phases of hepatic FFA synthesis the former phase was the malonyl-CoA increasing phase (lipog1) of 0.5-1.8 h, the latter

was its decreasing phase (lipog2) of 1.8-3.5 h. They corresponded to the glucose utilization and production phases. During the former phase, an increase in pyruvate enhanced malonyl-CoA production (**Figure 2**), while a decrease in G6P reduced the pentose phosphate pathway flux and NADPH production. Since NADPH, which is required for the conversion from malonyl-CoA to FFA (lipog2), was decreased, malonyl-CoA was accumulated. During the latter phase, an increase in G6P enhanced the pentose phosphate pathway flux and NADPH production. The accumulated malonyl-CoA was converted into FFA using NADPH. As shown in **Supplemental Figure S1**, the simulated Bhb production increased at the early phase of a fasted condition, as indicated by the experimental data (*56*), but it gradually decreased after 150 h with a decrease in plasma FFA, which was not consistent with the experimental data that gradually increased with time. The decrease in the simulated Bhb production under the fasted condition can be divided into the two phases: the former phase that both GI and adipose tissue secrete FFA and the latter phase that only adipose tissue releases FFA due to depleted TG in GI. We need to uncover novel mechanisms increasing plasma FFA under the fasted condition.

Pathological analysis

Individual disorders

The proposed model was used to perform pathological analysis of metabolic diseases. First I simulated the effects of the individual disorders on marker metabolites such as plasma glucose, plasma insulin and hepatic TG, as shown in **Figure 8ABC**. In general, high plasma glucose and hepatic TG accumulation develop or exacerbate metabolic diseases (*13, 15*). In the steatosis model, hepatic TG increased due to acceleration of lipogenesis. Cholesterol synthesis also increased in liver (data not shown), while the dynamics of plasma insulin and plasma glucose were almost the same as that of the normal condition. In β cell dysfunction of pancreas, where glucose-stimulated insulin secretion function is impaired or Km_inssyn_Glc_B is increased, the plasma insulin concentration decreased; the peak and set-point of plasma glucose increased. Plasma glucose was less utilized by liver, skeletal muscle and adipose tissue due to the impaired insulin secretion. Interestingly, hepatic TG decreased, which conflicted with the fact that the β cell dysfunction exacerbates the diseases. Type 1 diabetes is an extreme case of the β cell dysfunction, where Km_inssyn_Glc_B approaches to infinity or insulin is hardly produced in pancreas.

IR_L increased the peak and set-point of plasma glucose. Hyperinsulinemia, which is a compensatory response to IR (*58, 59*), was observed, as indicated by the experimental data (*58*). Plasma glucose dropped after 8 h due to reduced glycogenesis. It is because IR_L reduces the hepatic glycogen synthesis, resulting in insufficient accumulation of glycogen after the meal (data not shown). Interestingly, hepatic TG decreased, which presents a paradox or conflict that IR_L recovers hepatic steatosis or ectopic TG accumulation that is a major cause of IR_L (*16*). IR_M increased the peak and set-point of plasma glucose slightly. The plasma insulin slightly increased due to hyperglycemia. IR_M increased TG and DNL (data not shown) in liver. While skeletal muscle decreased the uptake of plasma glucose due to IR_M, liver utilized glucose for DNL in response to hyperinsulinemia and hyperglycemia. It indicates that plasma glucose is diverted away from muscle glycogen storage to hepatic TG. IR_A hardly increased the set-point of plasma glucose, while increasing hepatic TG and DNL in liver (data not shown). It is because insulin-regulated TG synthesis in adipose tissue is repressed and lipolysis is

enhanced. The increased plasma FFA enters liver to synthesize TG.

Combined disorders

The proposed model was applied to pathological analysis for type 2 diabetes. Particularly, I analyzed the effect of IR on progression of type 2 diabetes. I added the single disorders of IR_M, IR_A, and IR_L one by one to the base model consisting of steatosis and β cell dysfunction, as shown in **Figure 8DEF**. Addition of IR_M to the steatosis and β cell dysfunction base model decreased plasma insulin and increased the peak and set-point of plasma glucose more than that of the normal condition, indicating hyperglycemia. IR_M decreased the glucose uptake by skeletal muscle, increasing hepatic TG. When IR_A was added to the steatosis, β cell dysfunction and IR_M model, the plasma insulin and glucose hardly changed; hepatic TG increased due to the enhanced release of FFA from adipose tissue. Addition of IR_L further increased the set-point of plasma glucose, while increasing plasma insulin. Interestingly, it decreased hepatic TG.

Medication analysis

The proposed model was employed to investigate how three medicines of widely prescribed type 2 diabetes of sulfonylurea, metformin and thiazolidinedione and a glycerol kinase inhibitor recover type 2 diabetes, as shown in **Figure 9ABC**. Sulfonylurea administration successfully decreased plasma glucose with an increase in plasma insulin, but increased hepatic TG as a side effect. Metformin not only act on LDH but also β-oxidation through AMPK. The LDH inhibition by metformin decreased plasma glucose and hepatic TG, while increasing plasma lactate (data not shown). Activation of β-oxidation by metformin decreased hepatic TG without changing plasma glucose. Thiazolidinedione activated TG synthesis in adipose tissue, which decreased hepatic TG and hardly changed plasma glucose. Administration of a glycerol kinase inhibitor decreased hepatic TG accumulation. Unexpectedly, it decreased plasma glucose. The glycerol kinase inhibitor was referred to as a drug candidate that cures type 2 diabetes.

Design of combination therapy

To investigate the feasibility of combination therapy, I employed three medicines (metformin, thiazolidinedione and sulfonylurea) and a glycerol kinase inhibitor. **Figure 9DEF** shows the simulation results of three combination therapies. Expectedly metformin decreased plasma glucose and hepatic TG. The combination of metformin and thiazolidinedione additively decreased hepatic TG; it hardly changed the insulin and glucose dynamics. Addition of the glycerol kinase inhibitor to the two medicines further decreased plasma glucose and hepatic TG; it hardly changed the insulin concentration. The combination of all the four compounds further decreased plasma glucose, while increasing plasma insulin (by sulfonylurea). It hardly changed hepatic TG compared to the combination of metformin, thiazolidinedione, and glycerol kinase inhibitor. These simulation results revealed that the combination therapy is effective in reducing plasma glucose and hepatic TG. The combination therapy presented explicitly additive effects because the four medicine acted on different reactions.

DISCUSSION

Modular model construction

I have constructed a computational model that integrated eight organ modules and formulates the whole-body metabolism at the three scales of body, organ, and molecule. It is the most comprehensive and highly predictive model of the human metabolism. All the organ modules are connected through blood. The divide and conquer strategy at the organ scale allows us to run the individual organs separately and to exchange organs without any extensive rework at other scales. This modular dynamic model accurately reproduced the dynamics of experimental data of insulin, glucose, lactate, FFA, and TG concentrations and transport/exchange fluxes between blood and other organs after a meal and at rest. This model captured key features of human-whole body metabolism: lactate-glucose, alanine-glucose, glycerol-glucose cycles between liver and other organs. The model reproduced the two typical features of DNL suppressing β-oxidation and of glycolysis or PDH reaction decreasing β-oxidation. The former is effective in avoiding their futile cycles; the latter is effective in adjusting the energy balance between glycolysis and β-oxidation. In addition, the model presented a critical switching function between DNL and Bhb synthesis with respect to pyruvate in liver (**Figure 5)**. Pyruvate played a critical role in determining the entry of acetyl-CoA into TCA cycle, DNL or synthesis of FFA from citrate (CIT), and Bhb synthesis. Since the entry reaction of the TCA cycle in mitochondria is presented by oxaloacetate (OAA)+acetyl-CoA->CIT, OAA that comes from pyruvate is essential to drive the TCA reaction. Shortage of pyruvate, which decreases the supply of OAA, suppresses the entry reaction of the TCA cycle. When plasma glucose decreases under a fasted condition, a low glycolysis flux causes shortage of pyruvate or repression of the TCA cycle. In this case, β-oxidation-produced acetyl-CoA is not consumed by the TCA cycle, but utilized for the synthesis of Bhb. On the other hand, at high plasma glucose, abundant pyruvate activates the TCA cycle flux, enhancing CIT production in mitochondria. The CIT is transported into cytoplasm, converted into acetyl-CoA, a precursor of FFA synthesis. Consequently, high plasma glucose enhances DNL.

I discuss some discrepancies between experimental data and simulation. This model reproduced the experimental plasma glucose pulse, but did not exactly reproduce the experimental insulin pulse. It was inevitable in this model, because the insulin dynamics was tightly coupled with the glucose pulse (**Supplemental Equation S4**). The insulin pulse was tailed probably due to some hidden mechanisms. The simulated glycogen concentration in liver increased to a peak 2-3 h before experimental peak, and it decreased more rapidly than experimental data. The fast glycogen synthesis may result from the assumption that the model lumps many reactions involved in glycogen synthesis. The fast degradation may be caused by the fact that the model does not include kidney. Kidney is known to release glucose after the meal, which facilitates substantial liver glycogen repletion or suppression of glycogenolysis (*60*). In addition, the model simulated a gradual decrease in Bhb production after 150 h (**Supplemental Figure S1**), which was opposite to the experimental time course data indicating an increase in Bhb (*56*). It suggested some mechanisms enhancing FFA production in a fasted condition.

Model validity

The employed experimental data were a collection of different references, i.e., the experimental data were not obtained under the exactly same conditions. For example, the time course data of plasma insulin, plasma glucose, and plasma lactate derived from (*40*),

while the experimental data of their transport fluxes came from (*4*). The proposed model did not insist on the exact fitting, but pursued capturing critical metabolic features. In human metabolism studies, direct measurements of *in vivo* kinetics are very hard and *in vivo* experiments are seriously limited due to ethical issues. Since it is difficult to obtain a sufficient amount of data for kinetic modeling at present and in the near future, we have to manage fragmental, heterogeneous quantitative data, qualitative data, and biological knowledge to build a mathematical model (*38, 39*). The important thing is not to precisely measure or evaluate the exact values of kinetic parameters, but to capture essential functions underlying metabolic networks without insisting on the exact values *in vivo* nor on complexity in detailed biochemistry (*61, 62*).

I derived the rate equations from precise chemical reaction equations (*33*) when the experimentally validated equations are not available. Due to shortage of measured data, I did not uniquely determine the kinetic parameter values. However, existing experimental data including *in vitro* measured kinetic constants, qualitative data and biological information rather constrained the parameter space of the kinetic model. They were feasible enough for constructing kinetic models, for understanding the mechanisms by which the metabolic networks generate physiological functions and robustness, and for performing pathological and medication analysis. The resolution of the model is appropriate enough for the given experimental data and biological information. It may be no use to build much more detailed mathematical equations, if there is little experimental data to validate them.

Robustness

I discuss the dynamic sensitivity of metabolite concentrations with respect to a kinetic parameter. Generally, high sensitivity-providing parameters point out critical mechanisms such as ultrasensitivity, positive feedback loop, and bottleneck reactions. The insulin-related kinetic parameters of Km_inssyn_Glc_B, Km_Ins_B_L and Km_Ins_B_M showed high sensitivity, because they were employed by Hill equations providing ultrasensitivity. Such ultrasensitivity makes it possible for insulin to induce the distinct shift between glucose utilization and production. The coenzyme (ATP, GTP, UTP, NADH, NADPH, and $FADH_2$) synthesis-related parameters greatly affected the major pathways of β-oxidation, TCA cycle, and PDH reaction, while previous whole-body models hardly considered nucleotide cofactors (*4, 28, 29*). NAD^+ affects the reactions of TCA cycle, β-oxidation, LDH, and glyceraldehyde-3-phosphate dehydrogenase (G3PD). G3PD is the critically responsible enzyme for linking glycolysis to TG synthesis. NADH, which is produced through glycolysis, β-oxidation, and TCA cycle, is essential to generate ATP through oxidative phosphorylation. NADPH, which is produced in the pentose phosphate pathway, is utilized for DNL. UTP, which is essential for glycogen synthesis, is regenerated by nucleotide diphosphate kinase reaction of ATP +UDP-> ADP + UTP. GTP, which is necessary for gluconeogenesis (**Figure 2**), is also regenerated by nucleotide diphosphate kinase reaction of ATP +GDP-> ADP + GTP. Those nucleotide cofactors conjugate multiple cofactor-coupled reactions to form global positive feedback loops, which is exemplified by glycolysis pathways with TCA cycle and oxidative phosphorylation (*63, 64*). Glycolysis requires ATP at the initial step (HK, PFK) (**Figure 2**). An increase in glycolysis flux enhances the TCA cycle with oxidative phosphorylation to further produce ATP, which activates the initial step of glycolysis in a positive feedback manner. This ATP amplification is called turbo-design or self-replenishment cycle (*63,*

64). It accelerates the glucose utilization (HK, PFK) to reduce plasma glucose. β-oxidation in each organ and Bhb degradation in brain also employ the similar positive feedback loops. Thus, incorporation of nucleotide cofactors is effective in understanding the mechanisms of global metabolic changes.

While the insulin-related parameters including Km_inssyn_Glc_B, Km_Ins_B_L and Km_Ins_B_M played a critical role in changing a set-point (5mM) of plasma glucose concentration, the set-point provided a highly robust property against changes in the other kinetic parameters. The set-point of plasma glucose is rigorously controlled by insulin. To confirm the robustness of the set-point, we boldly set Vdif_glut3_Glc_B_N = 0 to stop the glucose uptake by brain. Surprisingly, the set-point was held (data not shown) by the insulin-based feedback switching between glucose utilization and production in liver. In addition, nucleotide cofactors conjugate multiple cofactor-coupled reactions to generate global negative feedback loops. The negative loops control the balances of NADH redox energy and ATP energy. For example, an increase in NADH suppresses β-oxidation and PDH reaction, while inducing LDH reaction, due to the decreased NAD^+, which results in suppression of TCA cycle and NADH synthesis. Excess ATP would promote the synthesis of TG, cholesterol and glycogen, which consumes ATP.

Prediction of hidden mechanism

The proposed model suggested a two-phase mechanism of FFA synthesis in liver, which consists of the former malonyl-CoA accumulation phase; the latter malonyl-CoA decreasing phase (**Figure 6**). This separation is caused by the fact that NADPH synthesis in the pentose phosphate pathways is coupled with DNL (**Figure 2**). Malonyl-CoA is a key intermediate metabolite for the FFA synthesis. During the former phase, G6P in liver decreases, which decreases the pentose phosphate pathway flux and NADPH. Malonyl-CoA is accumulated due to shortage of NADPH. During the latter phase, G6P increases, which enhances the pentose phosphate pathway flux and NADPH. The accumulated malonyl-CoA is converted with NADPH into FFA. The two phases correspond to the glucose production and utilization phases. Consequently, the DNL occurs shortly after the glucose pulse.

Pathological analysis

A computer model has an advantage in analysis of the individual disorders and in understanding some mechanisms by which the individual ones are combined to cause complex pathologies. Metabolic diseases take a matter of years to develop, but short-term simulation is effective in considering some signs of such diseases and in capturing typical pathological features. NAFLD or one of the most common chronic liver disorders worldwide is the build-up of excess TG in liver cells. It covers a wide range of liver dysfunctions, ranging from simple steatosis to non-alcoholic steatohepatitis (NASH), liver cirrhosis, and hepatocellular carcinoma (*8, 14, 44*). NAFLD has strong association with type 2 diabetes, 90% of obese patients with type 2 diabetes have NAFLD. NAFLD with IR progression leads to type 2 diabetes (*16*). I considered that NAFLD is hepatic steatosis with some IRs, while I did not simulate NAFLD due to its broad definition.

The proposed kinetic model was applied to pathological analysis for diabetes (*8, 44, 65*). There are two types of diabetes: type 1 and type 2. In type 1 diabetes, little or no insulin is produced by pancreas. Type 2 diabetes is characterized by steatosis, IR and β cell

dysfunction. Of course steatosis is the underlying disease. I investigated the effect of IR and β cell dysfunction on diabetes progression. IR_A alone hardly increased the plasma glucose set-point. The set-point increased in the order of IR_M, IR_L, and β cell dysfunction. The β cell dysfunction is the first major contribution; the IR_L is the second major one; IR_M is the third major one. β cell dysfunction and IR_L induced serious progression. The small difference in the plasma glucose set-point between IR_A and IR_M reflects that skeletal muscle accounts for 80% of the whole insulin-mediated glucose uptake (*66-68*). Quantitative understanding of the mechanisms responsible for insulin-controlled glucose uptake in each disorder is useful to evaluate the contribution of each disorder to type 2 diabetes.

The simulation results supported the widely-recognized experimental data that IR_M and IR_A promote hepatic TG synthesis. However, **Figure 8** suggests a paradox or conflict that β cell dysfunction and IR_L, which are known to exacerbate diabetes, recover the steatosis or ectopic TG accumulation that is a major cause of IR. I solve the paradox as follows. When IR occurs, hepatic TG accumulation may be no longer controlled by insulin (*69, 70*), but be transformed into a chronic or irreversible state through oxidation, ER stress, and inflammation (*71*).

Medication and combination therapy

Medication is a very popular way to treat type 2 diabetes. Out of many medications, I employed the three medicines of metformin, thiazolidinedione, and sulfonylurea and a glycerol kinase inhibitor that act on different reactions. Curative remedies are to reduce plasma glucose and to decrease ectopic TG accumulation. The three compounds of metformin, thiazolidinedione, glycerol kinase inhibitor were predicted to be effective in reduction of plasma glucose or hepatic TG. The model demonstrated a side effect of metformin that increased plasma lactate as lactic acidosis (simulation data not shown), as described elsewhere (*46, 53*). Interestingly, the proposed model revealed that the glycerol kinase inhibitor decreased not only hepatic TG but also plasma glucose. The reduced plasma glucose results from the shortage of glycerol-3-phosphate. Specifically, the shortage of glycerol-3-phosphate decreases the backward reaction from GRP to GAP, which results in reduced gluconeogenesis. The glycerol kinase inhibitor is found to be a promising medicine for type 2 diabetes. Out of several medications, activation of β-oxidation, which burns FFA, can be a powerful remedy to cure type 2 diabetes, because it has an advantage in removing not only TG but also its precursors. Metformin acts on β-oxidation through AMPK activation, while its action is marginal. Thus, new medicines should be developed that effectively activate β-oxidation. Sulfonylurea successfully reduced plasma glucose, but increased hepatic TG, suggesting a limitation or side effect of sulfonylurea. The model not only accurately predicted the essential results of medications but also achieved a rational design of combination therapy. The combination therapy of metformin, thiazolidinedione, glycerol kinase inhibitor, and sulfonylurea was found to be a promising therapy to reduce plasma glucose and hepatic TG. The successful combination results from the fact that the four compounds act on different reactions. The enhanced TG synthesis by sulfonylurea, which is a side effect, was compensated by the other three compounds.

Model limitation

IR can be caused by ectopic TG accumulation (*16, 50*). Specifically, DAG activates PKCs, impairing insulin signaling in organs. In IR-inducing processes, the ratio of saturated FFA to monounsaturated FFA plays a major role in disease progression (*72*). Saturated FFA leads to inflammation, ER stress and apoptosis. Since the present model is neither able to consider DAG nor saturated FFA, more detailed models are necessary that consider the IR-inducing mechanisms. The proposed model seems a mono-stable model (I have not found any bistability yet in the model), while real disorders are often chronical and irreversible. Actually, accumulated TG may be aggregated and denatured due to inflammation, oxidation and ER stress to cause chronic and irreversible dysfunctions (*16*). Such irreversible disorders should be considered in the next model.

Standard model of virtual metabolic human

Due to shortage of *in vivo* human measured data, the regulatory mechanisms on each organ metabolism are poorly understood. Nevertheless, to quantitatively understand the whole-body human metabolism from the limited data, a biochemistry-based mathematical model is very useful and rapidly becoming feasible. The proposed biochemistry-based model including the regulation of enzyme activities, allosteric reactions, nucleotide coenzyme reactions, and hormonal actions was able to reproduce many critical features of the whole human-body metabolism at the molecular level. It can be a standard model of the virtual metabolic human for pathological analysis and therapy design. The virtual metabolic human model is a valuable complement to experimental biology and clinical studies, because *in vivo* research involves serious ethical and technical problems.

ACKNOWLEDGMENTS

This work was supported by the Grant-in-Aid for Scientific Research (B) (19H04208) from Japan Society for the Promotion of Science. I am grateful of K. Horimoto, K, Ogata, K. Nasu, H. Shikita and R. Yoshimori performing computer simulation and system analysis. The organ illustrations in Figure 1A are provided by freepik (https://jp.freepik.com) and ac-illust (https://www.ac-illust.com/).

AUTHOR'S CONTRIBUTION

The first author did everything.

CONFLICT OF INTEREST

Nothing declared.

REFERENCES

1. M. Viceconti, P. Hunter, The Virtual Physiological Human: Ten Years After. *Annu Rev Biomed Eng* **18**, 103-123 (2016).

2. I. Thiele *et al.*, A community-driven global reconstruction of human metabolism. *Nat Biotechnol* **31**, 419-425 (2013).

3. A. Noronha *et al.*, The Virtual Metabolic Human database: integrating human and gut microbiome metabolism with nutrition and disease. *Nucleic Acids Res* **47**, D614-D624 (2019).

4. J. Kim, G. M. Saidel, M. E. Cabrera, Multi-scale computational model of fuel homeostasis during exercise: effect of hormonal control. *Ann Biomed Eng* **35**, 69-90 (2007).

5. Y. Li *et al.*, Computational model of cellular metabolic dynamics: effect of insulin on glucose disposal in human skeletal muscle. *Am J Physiol Endocrinol Metab* **298**, E1198-1209 (2010).

6. M. Konig, S. Bulik, H. G. Holzhutter, Quantifying the contribution of the liver to glucose homeostasis: a detailed kinetic model of human hepatic glucose metabolism. *PLoS Comput Biol* **8**, e1002577 (2012).

7. J. P. Sluka *et al.*, A Liver-Centric Multiscale Modeling Framework for Xenobiotics. *PLoS One* **11**, e0162428 (2016).

8. W. B. Ashworth, N. A. Davies, I. D. Bogle, A Computational Model of Hepatic Energy Metabolism: Understanding Zonated Damage and Steatosis in NAFLD. *PLoS Comput Biol* **12**, e1005105 (2016).

9. N. Berndt, H. G. Holzhutter, Dynamic Metabolic Zonation of the Hepatic Glucose Metabolism Is Accomplished by Sinusoidal Plasma Gradients of Nutrients and Hormones. *Front Physiol* **9**, 1786 (2018).

10. N. Berndt, M. S. Horger, S. Bulik, H. G. Holzhutter, A multiscale modelling approach to assess the impact of metabolic zonation and microperfusion on the hepatic carbohydrate metabolism. *PLoS Comput Biol* **14**, e1006005 (2018).

11. N. Berndt *et al.*, HEPATOKIN1 is a biochemistry-based model of liver metabolism for applications in medicine and pharmacology. *Nat Commun* **9**, 2386 (2018).

12. K. N. Frayn, *Metabolic regulation: A human perspective*. (Willey-Blackwell, UK, 2010).

13. M. F. Xia, H. Bian, X. Gao, NAFLD and Diabetes: Two Sides of the Same Coin? Rationale for Gene-Based Personalized NAFLD Treatment. *Front Pharmacol* **10**, 877 (2019).

14. H. Kitade, G. Chen, Y. Ni, T. Ota, Nonalcoholic Fatty Liver Disease and Insulin Resistance: New Insights and Potential New Treatments. *Nutrients* **9**, (2017).

15. F. M. Ashcroft, P. Rorsman, Diabetes mellitus and the beta cell: the last ten years. *Cell* **148**, 1160-1171 (2012).

16. R. J. Perry, V. T. Samuel, K. F. Petersen, G. I. Shulman, The role of hepatic lipids in hepatic insulin resistance and type 2 diabetes. *Nature* **510**, 84-91 (2014).

17. A. R. Saltiel, New perspectives into the molecular pathogenesis and treatment of type 2 diabetes.

Cell **104**, 517-529 (2001).

18. H. Kitano, Grand challenges in systems physiology. *Front Physiol* **1**, 3 (2010).

19. R. Iyengar, S. Zhao, S. W. Chung, D. E. Mager, J. M. Gallo, Merging systems biology with pharmacodynamics. *Sci Transl Med* **4**, 126ps127 (2012).

20. T. Eissing *et al.*, A computational systems biology software platform for multiscale modeling and simulation: integrating whole-body physiology, disease biology, and molecular reaction networks. *Front Physiol* **2**, 4 (2011).

21. E. M. Maldonado *et al.*, Multi-scale, whole-system models of liver metabolic adaptation to fat and sugar in non-alcoholic fatty liver disease. *NPJ Syst Biol Appl* **4**, 33 (2018).

22. I. D. L. Bogle *et al.*, Systems Biology of the Liver. *Reviews in Cell Biology and Molecular Medicine*, (2012).

23. J. Hetherington *et al.*, A composite computational model of liver glucose homeostasis. I. Building the composite model. *J R Soc Interface* **9**, 689-700 (2012).

24. T. Sumner *et al.*, A composite computational model of liver glucose homeostasis. II. Exploring system behaviour. *J R Soc Interface* **9**, 701-706 (2012).

25. T. Pearson, J. A. Wattis, J. R. King, I. A. MacDonald, D. J. Mazzatti, A mathematical model of the human metabolic system and metabolic flexibility. *Bull Math Biol* **76**, 2091-2121 (2014).

26. A. C. Pratt, J. A. Wattis, A. M. Salter, Mathematical modelling of hepatic lipid metabolism. *Math Biosci* **262**, 167-181 (2015).

27. C. Z. W. Hassell Sweatman, Mathematical model of diabetes and lipid metabolism linked to diet, leptin sensitivity, insulin sensitivity and VLDLTG clearance predicts paths to health and type II diabetes. *J Theor Biol* **486**, 110037 (2020).

28. K. Xu, K. T. Morgan, A. Todd Gehris, T. C. Elston, S. M. Gomez, A whole-body model for glycogen regulation reveals a critical role for substrate cycling in maintaining blood glucose homeostasis. *PLoS Comput Biol* **7**, e1002272 (2011).

29. M. C. Palumbo *et al.*, Personalizing physical exercise in a computational model of fuel homeostasis. *PLoS Comput Biol* **14**, e1006073 (2018).

30. F. Q. Nuttall, A. Ngo, M. C. Gannon, Regulation of hepatic glucose production and the role of gluconeogenesis in humans: is the rate of gluconeogenesis constant? *Diabetes Metab Res Rev* **24**, 438-458 (2008).

31. L. J. Mandarino, A. Consoli, A. Jain, D. E. Kelley, Interaction of carbohydrate and fat fuels in human skeletal muscle: impact of obesity and NIDDM. *Am J Physiol* **270**, E463-470 (1996).

32. L. J. Mandarino, A. Consoli, A. Jain, D. E. Kelley, Differential regulation of intracellular glucose metabolism by glucose and insulin in human muscle. *Am J Physiol* **265**, E898-905 (1993).

33. N. Swainston *et al.*, Recon 2.2: from reconstruction to model of human metabolism. *Metabolomics* **12**, 109 (2016).

34. D. Kawamori *et al.*, Insulin signaling in alpha cells modulates glucagon secretion in vivo. *Cell Metab* **9**, 350-361 (2009).

35. D. Kawamori, M. Akiyama, J. Hu, B. Hambro, R. N. Kulkarni, Growth factor signalling in the regulation of alpha-cell fate. *Diabetes Obes Metab* **13 Suppl 1**, 21-30 (2011).

36. H. Kurata *et al.*, Extended CADLIVE: a novel graphical notation for design of biochemical network maps and computational pathway analysis. *Nucleic Acids Res* **35**, e134 (2007).

37. J. R. Karr *et al.*, A whole-cell computational model predicts phenotype from genotype. *Cell* **150**, 389-401 (2012).

38. K. Maeda, H. Minamida, K. Yoshida, H. Kurata, Flux module decomposition for parameter estimation in a multiple-feedback loop model of biochemical networks. *Bioprocess Biosyst Eng* **36**, 333-344 (2013).

39. K. Maeda, H. V. Westerhoff, H. Kurata, F. C. Boogerd, Ranking network mechanisms by how they fit diverse experiments and deciding on E. coli's ammonium transport and assimilation network. *NPJ Syst Biol Appl* **5**, 14 (2019).

40. K. N. Frayn, S. W. Coppack, S. M. Humphreys, M. L. Clark, R. D. Evans, Periprandial regulation of lipid metabolism in insulin-treated diabetes mellitus. *Metabolism* **42**, 504-510 (1993).

41. R. Taylor *et al.*, Direct assessment of liver glycogen storage by 13C nuclear magnetic resonance spectroscopy and regulation of glucose homeostasis after a mixed meal in normal subjects. *J Clin Invest* **97**, 126-132 (1996).

42. F. Karpe, T. Olivecrona, G. Walldius, A. Hamsten, Lipoprotein lipase in plasma after an oral fat load: relation to free fatty acids. *J Lipid Res* **33**, 975-984 (1992).

43. H. Masunaga *et al.*, Robustness analysis of the detailed kinetic model of an ErbB signaling network by using dynamic sensitivity. *PLoS One* **12**, e0178250 (2017).

44. J. K. Dowman, J. W. Tomlinson, P. N. Newsome, Pathogenesis of non-alcoholic fatty liver disease. *QJM* **103**, 71-83 (2010).

45. J. Friedman, Fat in all the wrong places. *Nature* **415**, 268-269 (2002).

46. B. Molavi, N. Rassouli, S. Bagwe, N. Rasouli, A review of thiazolidinediones and metformin in the treatment of type 2 diabetes with focus on cardiovascular complications. *Vasc Health Risk Manag* **3**, 967-973 (2007).

47. F. Guebre-Egziabher *et al.*, Ectopic lipid accumulation: A potential cause for metabolic disturbances and a contributor to the alteration of kidney function. *Biochimie* **95**, 1971-1979 (2013).

48. E. R. Gilbert, D. Liu, Epigenetics: the missing link to understanding beta-cell dysfunction in the pathogenesis of type 2 diabetes. *Epigenetics* **7**, 841-852 (2012).

49. G. C. Yaney, B. E. Corkey, Fatty acid metabolism and insulin secretion in pancreatic beta cells. *Diabetologia* **46**, 1297-1312 (2003).

50. M. E. Cerf, Beta cell dysfunction and insulin resistance. *Front Endocrinol (Lausanne)* **4**, 37 (2013).

51. W. K. Seltzer, G. Dhariwal, H. A. McKelvey, E. R. McCabe, 1-Thioglycerol: inhibitor of glycerol kinase activity in vitro and in situ. *Life Sci* **39**, 1417-1424 (1986).

52. C. L. Aquilante, Sulfonylurea pharmacogenomics in Type 2 diabetes: the influence of drug target and diabetes risk polymorphisms. *Expert Rev Cardiovasc Ther* **8**, 359-372 (2010).

53. I. Pernicova, M. Korbonits, Metformin--mode of action and clinical implications for diabetes and cancer. *Nat Rev Endocrinol* **10**, 143-156 (2014).

54. M. D. Fullerton *et al.*, Single phosphorylation sites in Acc1 and Acc2 regulate lipid homeostasis and the insulin-sensitizing effects of metformin. *Nat Med* **19**, 1649-1654 (2013).

55. N. Rasouli *et al.*, Pioglitazone improves insulin sensitivity through reduction in muscle lipid and redistribution of lipid into adipose tissue. *Am J Physiol Endocrinol Metab* **288**, E930-934 (2005).

56. O. E. Owen, L. Tappy, M. A. Mozzoli, K. J. Smalley, in *The metabolic and molecular basis of acquired disease,* R. D. Cohen, B. Lewis, K. G. M. M. Alberti, A. M. Denman, Eds. (Bailliere Tindall, London, 1990), vol. 1, pp. 550-570.

57. J. Jensen, P. I. Rustad, A. J. Kolnes, Y. C. Lai, The role of skeletal muscle glycogen breakdown for regulation of insulin sensitivity by exercise. *Front Physiol* **2**, 112 (2011).

58. R. A. DeFronzo, D. Tripathy, Skeletal muscle insulin resistance is the primary defect in type 2 diabetes. *Diabetes Care* **32 Suppl 2**, S157-163 (2009).

59. K. F. Petersen *et al.*, The role of skeletal muscle insulin resistance in the pathogenesis of the metabolic syndrome. *Proc Natl Acad Sci U S A* **104**, 12587-12594 (2007).

60. C. Meyer, J. M. Dostou, S. L. Welle, J. E. Gerich, Role of human liver, kidney, and skeletal muscle in postprandial glucose homeostasis. *Am J Physiol Endocrinol Metab* **282**, E419-427 (2002).

61. H. Kurata, K. Masaki, Y. Sumida, R. Iwasaki, CADLIVE dynamic simulator: direct link of biochemical networks to dynamic models. *Genome Res* **15**, 590-600 (2005).

62. H. Kurata, N. Matoba, N. Shimizu, CADLIVE for constructing a large-scale biochemical network based on a simulation-directed notation and its application to yeast cell cycle. *Nucleic Acids Res* **31**, 4071-4084 (2003).

63. H. Kurata, Self-replenishment cycles generate a threshold response. *Sci Rep* **9**, 17139 (2019).

64. B. Teusink, M. C. Walsh, K. van Dam, H. V. Westerhoff, The danger of metabolic pathways with turbo design. *Trends Biochem Sci* **23**, 162-169 (1998).

65. K. M. Utzschneider, S. E. Kahn, Review: The role of insulin resistance in nonalcoholic fatty liver disease. *J Clin Endocrinol Metab* **91**, 4753-4761 (2006).

66. A. R. Saltiel, C. R. Kahn, Insulin signalling and the regulation of glucose and lipid metabolism. *Nature* **414**, 799-806 (2001).

67. C. S. Stump, E. J. Henriksen, Y. Wei, J. R. Sowers, The metabolic syndrome: role of skeletal muscle metabolism. *Ann Med* **38**, 389-402 (2006).

68. F. S. Thong, C. B. Dugani, A. Klip, Turning signals on and off: GLUT4 traffic in the insulin-signaling highway. *Physiology (Bethesda)* **20**, 271-284 (2005).

69. J. K. Kim *et al.*, Tissue-specific overexpression of lipoprotein lipase causes tissue-specific insulin resistance. *Proc Natl Acad Sci U S A* **98**, 7522-7527 (2001).

70. H. Doege *et al.*, Silencing of hepatic fatty acid transporter protein 5 in vivo reverses diet-induced non-alcoholic fatty liver disease and improves hyperglycemia. *J Biol Chem* **283**, 22186-22192 (2008).

71. P. Ferre, F. Foufelle, Hepatic steatosis: a role for de novo lipogenesis and the transcription factor SREBP-1c. *Diabetes Obes Metab* **12 Suppl 2**, 83-92 (2010).

72. N. Alkhouri, L. J. Dixon, A. E. Feldstein, Lipotoxicity in nonalcoholic fatty liver disease: not all lipids are created equal. *Expert Rev Gastroenterol Hepatol* **3**, 445-451 (2009).

A

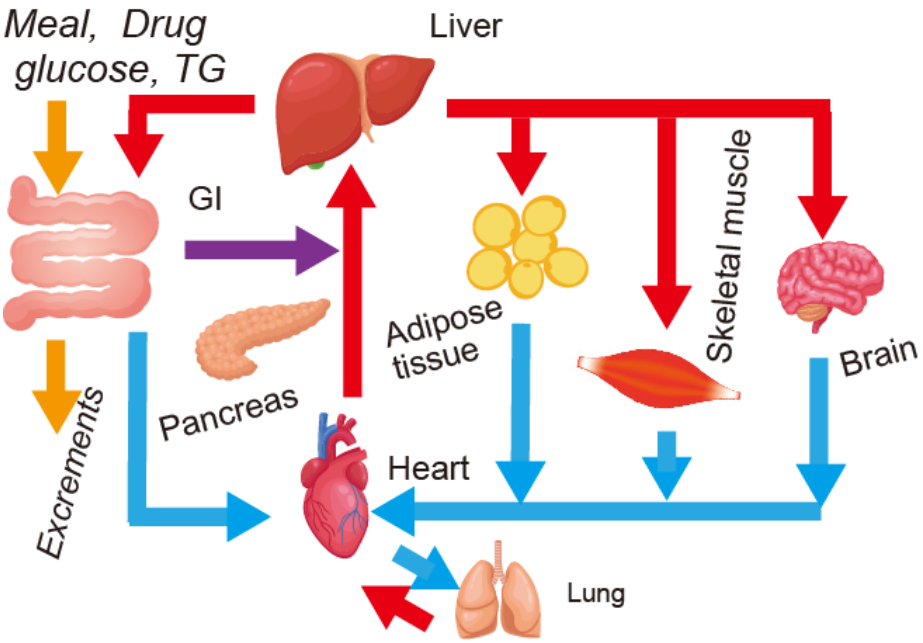

B

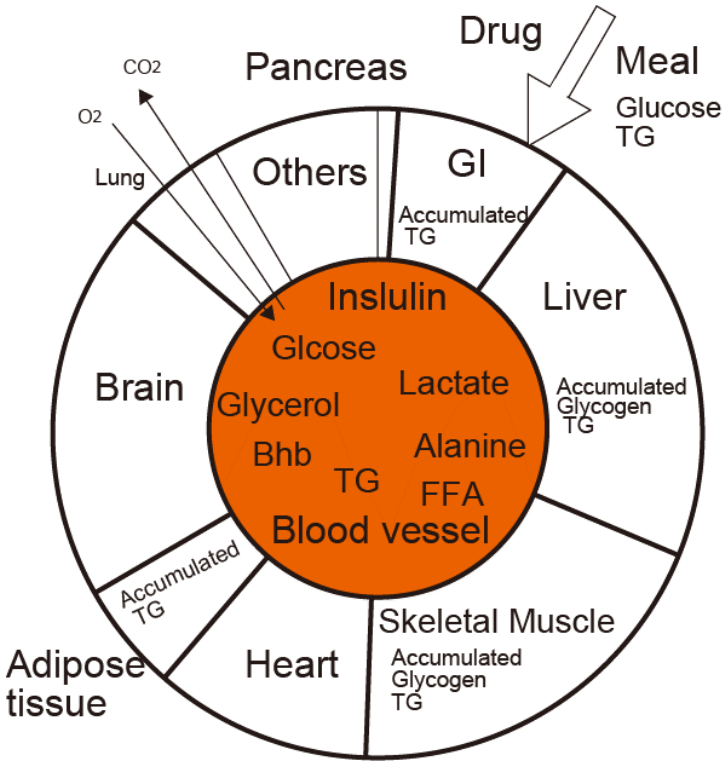

Figure 1 Schematic diagram of the human whole-body metabolism.

(A) Realistic multi-organ model. (B) Perfect mixing model of the whole body

Oxygen and carbon dioxide concentrations are assumed to be constant in the whole body, thus the kinetic model does not include lung and them.

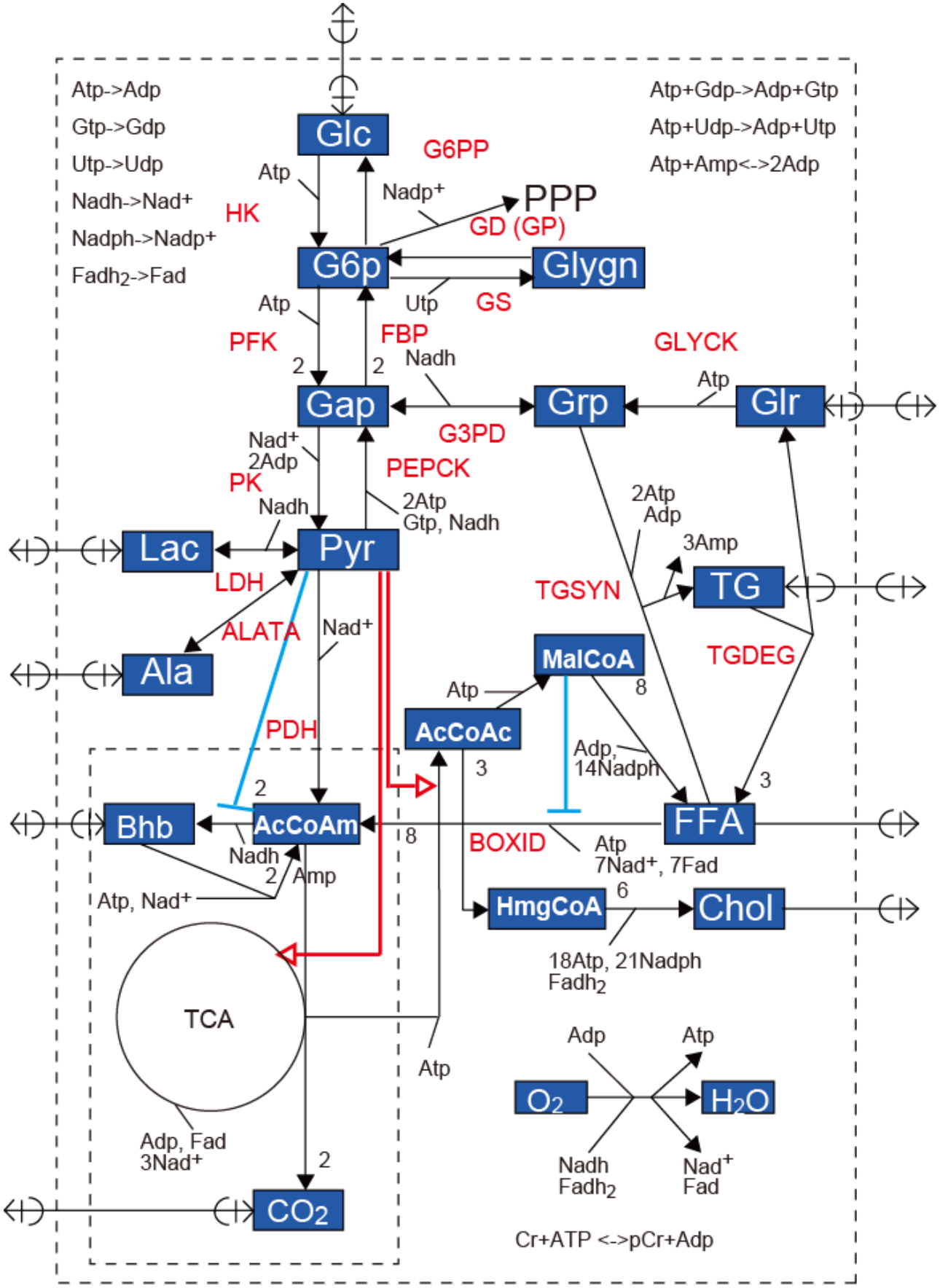

Figure 2 Union map of all organ metabolic networks

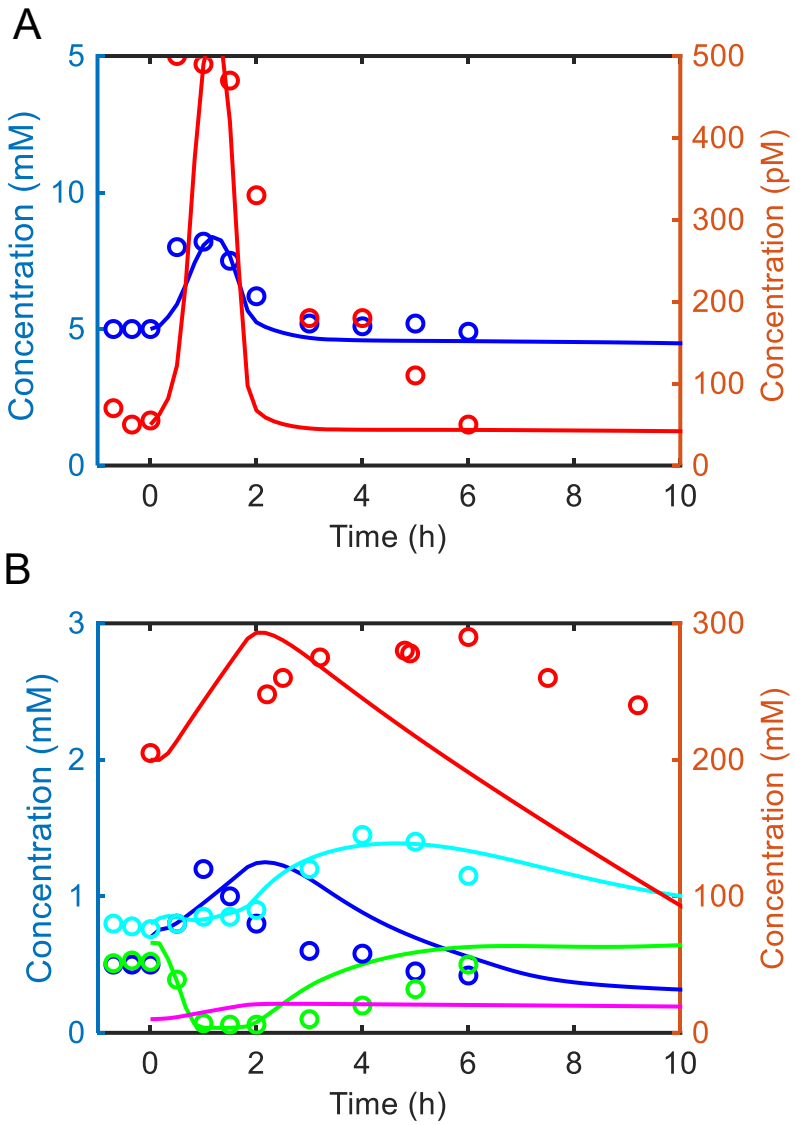

Figure 3 Time course of key metabolites in blood, liver and skeletal muscle after an overnight fast and following a single meal of 100 g glucose and 33 g fat.

(A) Circles and lines indicate the experimental and simulated concentrations of plasma glucose (blue) and insulin (red), respectively.

(B) Circles and lines indicate the experimental and simulated concentrations of plasma lactate (blue), plasma FFA (green), plasma TG (cyan), hepatic glycogen (red) and skeletal muscle glycogen (magenta).

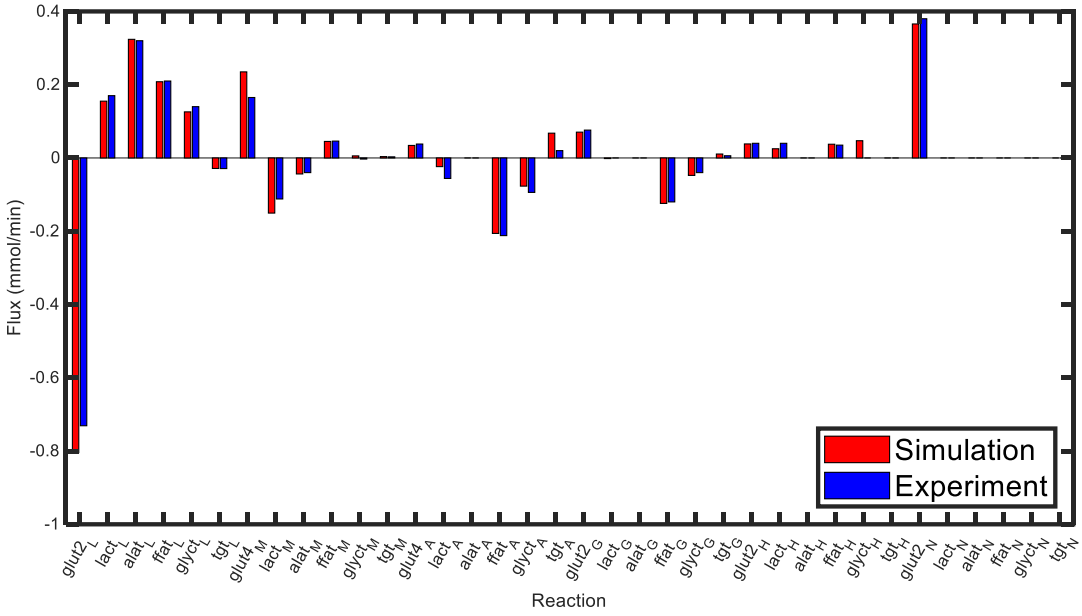

Figure 4 Transport/exchange fluxes at rest between blood and each organ.
Red and blue bars indicated the simulated and experimental fluxes, respectively.

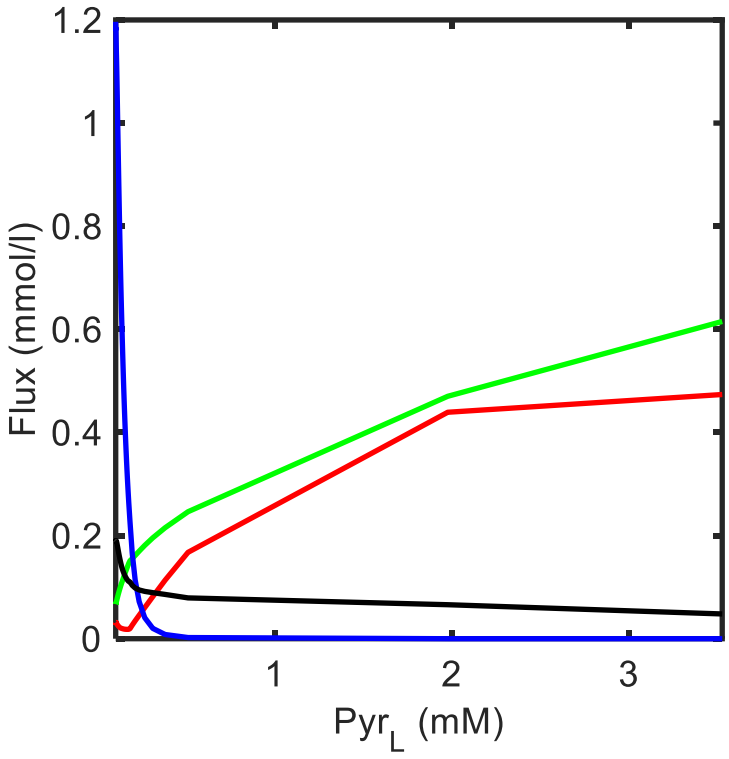

Figure 5 Changes in the simulated fluxes of key reactions with respect to hepatic pyruvate.

The proposed model was simulated during 480 h after an overnight fast and following a single meal of 100 g glucose and 33 g fat. The four fluxes of the PDH reaction (red), DNL (green), Bhb synthesis (blue), and β-oxidation (black) were plotted with respect to pyruvate concentration in liver.

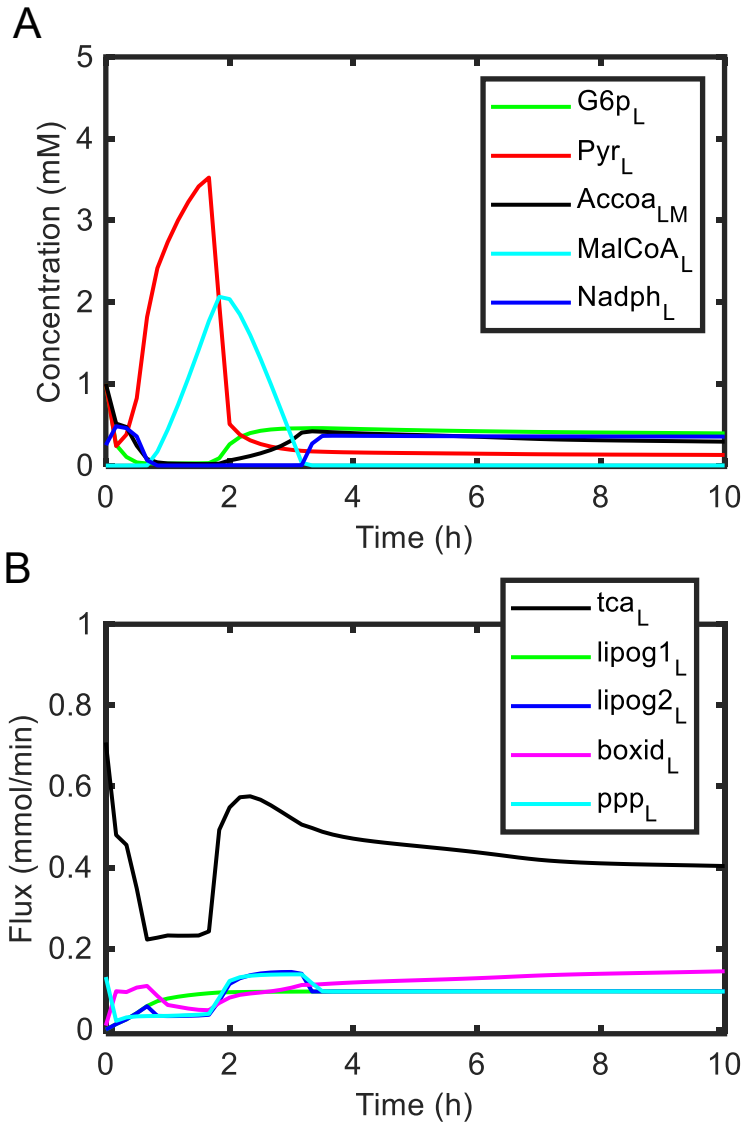

Figure 6 Prediction of a two-phase mechanisms of *de novo* lipogenesis in liver

The proposed model was simulated during 10 h after an overnight fast and following a single meal of 100 g glucose and 33 g fat.

(A) The time course of G6P (green), pyruvate (red), acetyl-CoA (black), malonyl-CoA (cyan) and NADPH (blue) concentrations were simulated.

(B) The time course of TCA cycle (black), lipog1(green), lipog2 (blue), β-oxidation (magenta) and pentose phosphate pathway (cyan) fluxes were simulated. The lipog1 and lipog2 indicate the conversion from acetyl-CoA to malonyl-CoA and the conversion from malonyl-CoA to FFA, respectively.

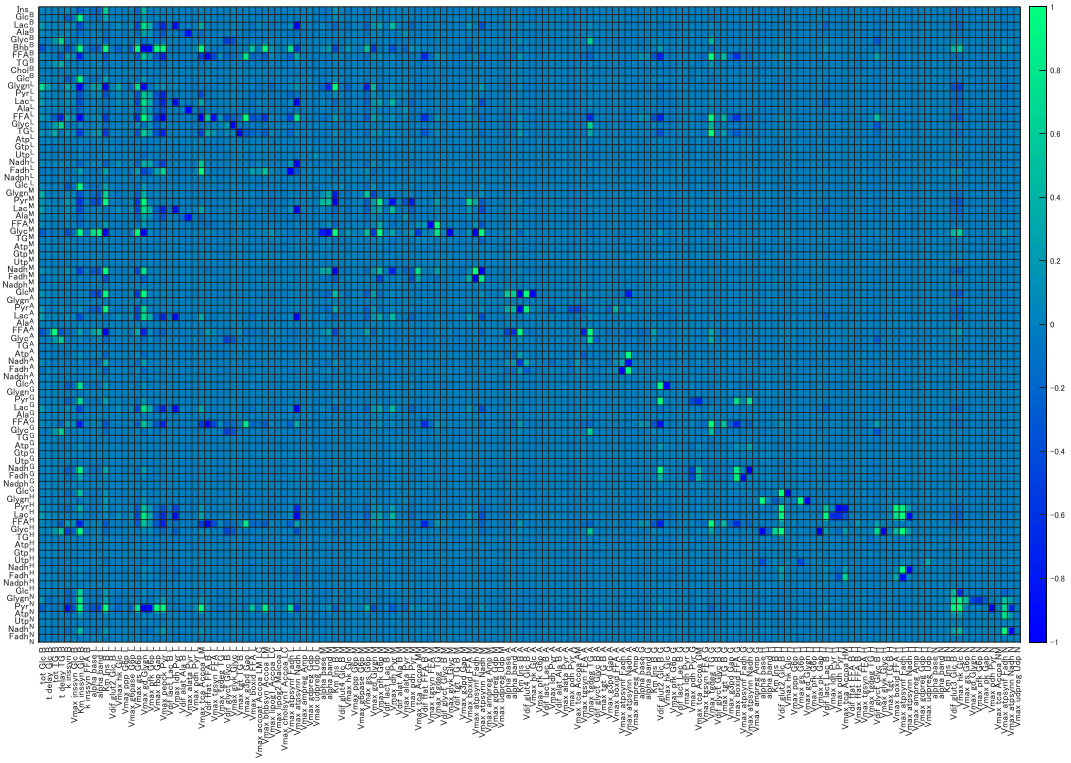

Figure 7 Dynamic sensitivity analysis of metabolite concentrations at rest with respect to a kinetic constant

The proposed model was simulated during 10 h after an overnight fast and following a single meal of 100 g glucose and 33 g fat, while changing the value of each kinetic parameter by 1.1-fold. The dynamic sensitivity was calculated at 10 h.

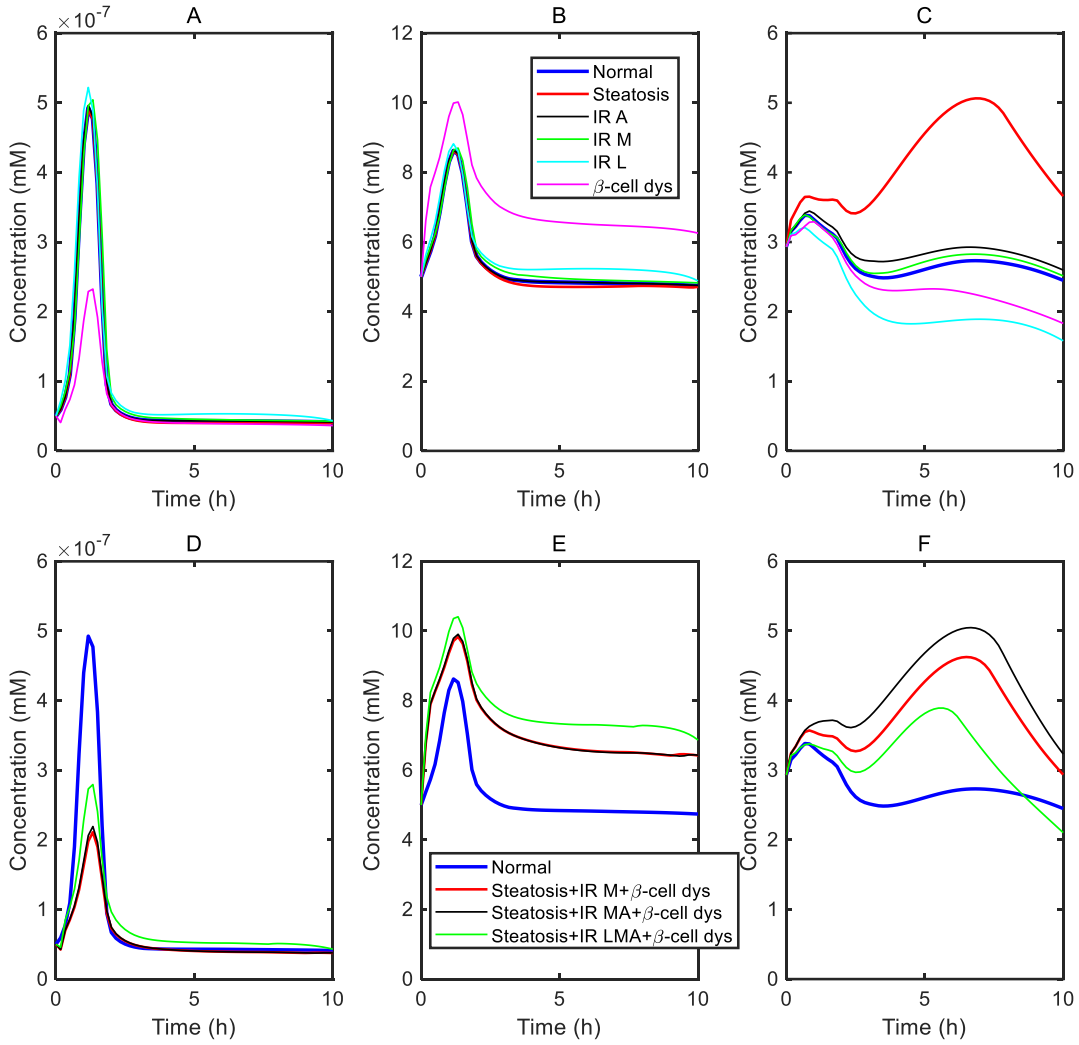

Figure 8 Pathological analysis using the proposed kinetic model.

(A-C) Single disorder. Time courses of plasma insulin (A), plasma glucose (B), and hepatic TG (C) for each disorder were simulated after an overnight fast and following a single meal of 100g glucose and 33 g TG. The lines indicate the normal condition (blue), steatosis (red), IR_A (black), IR_M (green), IR_L (cyan), and β-cell dysfunction (magenta).

Specifically, steatosis is built by multiplying Vmax_accoat_Accoa_LM_LC, Vmax_lipog1_Accoa_LC, Vmax_lipog2_Malcoa_L, and Vmax_tgsyn_FFA_L, Vmax_cholsyn1_Accoa_LC by 2. β-cell dysfunction is built by multiplying Km_inssyn_Glc_B by 1.5. IR_A is built by multiplying Km_Ins_B_A by 1.5. IR_M is built by multiplying Km_Ins_B_M by 1.5. IR_L is built by multiplying Km_Ins_B_L by 1.5.

(D-F) Combined disorders. Time courses of plasma insulin (D), plasma glucose (E), and hepatic TG (F) for each combined disorder model were simulated after an overnight fast and following a single meal of 100g glucose and 33 g TG. The lines indicate normal condition (blue), the combination of steatosis, β-cell dysfunction and IR_M (red), the combination of steatosis, β-cell dysfunction, IR_M, and IR_A (black), and the combination of steatosis, β-cell dysfunction, IR_M, IR_A, and IR_L (green).

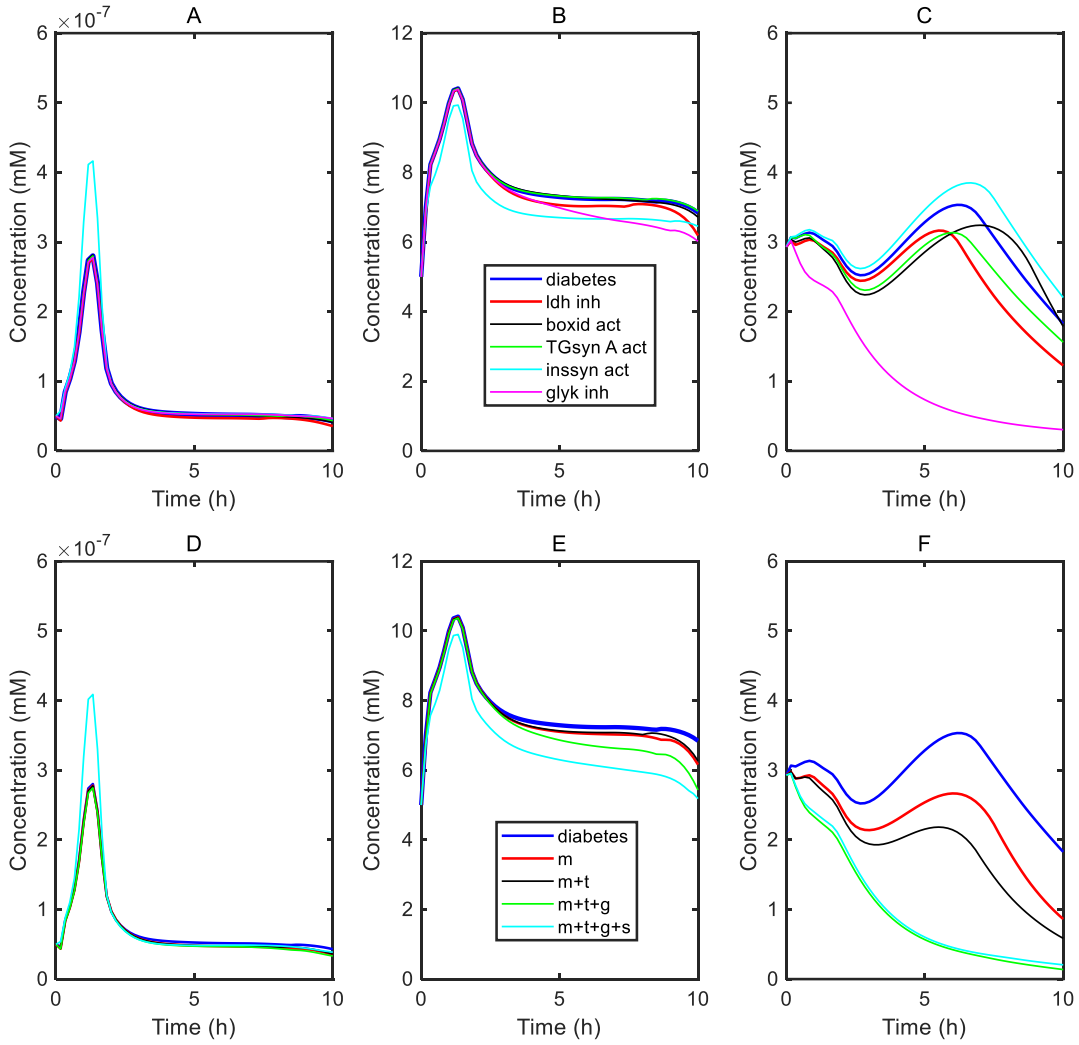

Figure 9 Single medication analysis and prediction of combination therapy for type 2 diabetes by using the proposed model.

(A-C) Single medication: Time courses of the concentration of plasma insulin (A), plasma glucose (B), and hepatic TG (C) for type 2 diabetes were simulated after an overnight fast and following a single meal of 100g glucose and 33 g TG. The lines indicate the type 2 diabetes model without any medication (blue), LDH inhibition by metformin (red), β-oxidation activation by metformin (black), thiazolidinedione (green), sulfonylurea (cyan), and glycerol kinase inhibitor (magenta). The type 2 diabetes model is the same as the green line of Figure 8DEF. Specifically, metformin reduces Vmax_ldh_Pyr_L to zero or multiplies Vmax_boxid_FFA_L by 2. Thiazolidinedione multiplies Vmax_tgsyn_FFA_A by 2. Sulfonylurea multiples Vmax_inssyn_Glc_B by 2. Glycerol kinase inhibitor reduces Vmax_glyk_Glyc_L to zero.

(D-F) Combination therapy: Time courses of the concentration of plasma insulin (D), plasma glucose (E), and hepatic TG (F) for type 2 diabetes were simulated after an overnight fast and following a single meal of 100g glucose and 33 g TG. The lines indicate no medication (blue), metformin (red), the combination of metformin and thiazolidinedione (black), the combination of metformin, thiazolidinedione and glycerol kinase inhibitor (green), and the combination of metformin, thiazolidinedione, glycerol kinase inhibitor, and sulfonylurea (cyan).